Flow-Regulated Growth of Titanium Dioxide (TiO_2) Nanotubes in Microfluidics

*Rong Fan, Xinye Chen, Zihao Wang, David Custer, and Jiandi Wan**

***E**lectrochemical anodization of titanium (Ti) in a static, bulk condition is used widely to fabricate self-organized TiO_2 nanotube arrays. Such bulk approaches, however, require extended anodization times to obtain long TiO_2 nanotubes and produce only vertically aligned nanotubes. To date, it remains challenging to develop effective strategies to grow long TiO_2 nanotubes in a short period of time, and to control the nanotube orientation. Here, it is shown that the anodic growth of TiO_2 nanotubes is significantly enhanced (≈16–20 times faster) under flow conditions in microfluidics. Flow not only controls the diameter, length, and crystal orientations of TiO_2 nanotubes, but also regulates the spatial distribution of nanotubes inside microfluidic devices. Strikingly, when a Ti thin film is deposited on silicon substrates and anodized in microfluidics, both vertically and horizontally aligned (relative to the bottom substrate) TiO_2 nanotubes can be produced. The results demonstrate previously unidentified roles of flow in the regulation of growth of TiO_2 nanotubes, and provide powerful approaches to effectively grow long, oriented TiO_2 nanotubes, and construct hierarchical TiO_2 nanotube arrays on silicon-based materials.*

TiO_2 nanotubes are of great importance in photocatalysis, solar cells, sensors, and other applications.[1–5] Self-organized TiO_2 nanotube arrays are commonly produced via electrochemical anodization of Ti, where a complex electric-field-aided oxidation and dissolution process is responsible for the formation of TiO_2 nanotube arrays.[6–14] Specifically, the oxidation of Ti at the anode produces Ti^{4+} ions that migrate under the electric field and react with O^{2-} ions to form the anodic TiO_2 layer. Fluoride (F^-) in the electrolyte, on the other hand, attacks the TiO_2 layer and generates water soluble TiF_6^{2-} ions, resulting in dissolution of the TiO_2 layer and initiates the formation of TiO_2 nanotube arrays. Although the reason why nanotubes, instead of a porous TiO_2 layer, are formed during anodization is debated,[7,9] TiO_2 nanotubes keep growing until the formation and dissolution of TiO_2 reach an equilibrium. At this stage, TiO_2 nanotubes are penetrating deeper into the metal to grow; however, nanotubes at the electrolyte–oxide interface dissolve at the same rate as growth, such that the thickness of the TiO_2 nanotube arrays, i.e., the length of TiO_2 nanotubes, remains constant. Because the growth of TiO_2 nanotubes is controlled by the field-aided oxidation and F^--based chemical dissolution, the diameter and length of TiO_2 nanotubes can be regulated by controlling the magnitude of an applied electrical field, composition of the electrolyte (i.e., concentration of F^-, pH, and water content), and anodization time.[7,12,15–17]

To date, most approaches to electrochemically produce TiO_2 nanotubes are conducted under static, bulk conditions with no or limited flow involved during anodization.[6–8] In this case, an initially formed, compact oxide layer with random pores often remains on the top of the TiO_2 nanotube arrays after anodization.[18–22] Although the existence of the compact oxide layer significantly limits the growth and application of TiO_2 nanotubes, effective removal of the compact oxide layer is difficult.[7,23,24] In addition, extended anodization time, which is required to produce long TiO_2 nanotubes, frequently leads to inhomogeneous tube diameter and structure due to the F^--based chemical etching process.[25,26] Introducing hydrodynamic factors such as stirring to the electrolyte solution during anodization increases the length of

R. Fan, X. Chen, Z. Wang, D. Custer, Dr. J. Wan
Microsystems Engineering
Rochester Institute of Technology
168 Lomb Memorial Drive, Rochester, NY 14623, USA
E-mail: jdween@rit.edu

DOI: 10.1002/smll.201701154

TiO_2 nanotubes up to 60%;[16] the flow, however, is not well-controlled, and the morphological homogeneity of nanotubes is negatively affected. To date, it remains technically challenging to grow long and homogeneous TiO_2 nanotubes in a short period of time. In addition, TiO_2 nanotubes produced under static and bulk conditions are all vertically aligned relative to the bottom substrate and there is no control over the spatial orientation of TiO_2 nanotubes.

Here, we describe a microfluidic approach to electrochemically grow TiO_2 nanotube arrays under controlled flow conditions. We show that the presence of flow during anodization impacts significantly on the growth of TiO_2 nanotube arrays, and both the structural and material properties of TiO_2 nanotubes can be manipulated. Furthermore, we demonstrate a strategy to produce previously unrealized horizontally aligned TiO_2 nanotubes in microfluidics. Our results highlight the importance of flow in the anodic growth of TiO_2 nanotube arrays, and the developed microfluidic approach provides an effective strategy to grow oriented TiO_2 nanotube arrays, and a powerful means to construct TiO_2-nanotube-based hierarchical structures.

The anodic growth of TiO_2 nanotubes was conducted in a Ti-based microfluidic device and characterized by scanning electron microscopy (SEM) (**Figure 1**A,B; Figure S1 and Table S1, Supporting Information). During anodization, we kept the applied voltage (40 V), composition of the electrolyte, and anodization time (30 min) constant for all microfluidic experiments, and only changed the hydrodynamic conditions in the microfluidic channel. Figure 1C shows a typical SEM image of the Ti microfluidic channel covered with TiO_2 nanotube arrays after anodization. Consistent with previous studies, there was a compact oxide layer on the top of the nanotube arrays (Figure S2, Supporting Information).[18–20] With an increase of flow rate, however, the thickness and the coverage of the compact oxide layer initially formed at the electrolyte–oxide interface decreased significantly (Figure 1D,E; Figure S2, Supporting Information), implying that high flow rate inhibits the formation of the compact oxide layer during anodization. In addition, although the outer diameter of the nanotube did not change significantly with flow rate, the inner diameter of the nanotube increased with flow rate (Figure 1F,H,I), resulting in a decrease of the wall thickness of the nanotube. Remarkably, the length of nanotubes increased up to ≈4000% as the flow rate increased from 0 to 200 µL min^{-1} (Figure 1G,J,K). The observed constant outer diameter at different flow rates is likely due to the constant anodization voltage,[10,27,28] whereas the change of inner diameter and length is due to the effect of flow on the dissolution process, which will be discussed in detail in the following sections.

It is important to note that the anodization time in the current microfluidic setup is 30 min, whereas it takes ≈8–10 h to grow similar length nanotubes in static, bulk conditions.[21,29] In addition, TiO_2 nanotubes produced under flow conditions have diameters with a narrow size distribution (Figure S3, Supporting Information), suggesting that flow does not lead to inhomogeneous top structures as observed in most long-duration anodization experiments.[22,26] Furthermore, when TiO_2 nanotubes were annealed at 425 °C and analyzed by X-ray diffraction (XRD), typical anatase TiO_2 reflection peaks at the (101), (004), and (200) surfaces were observed and the magnitude of the reflection peak increased with flow rate (Figure 1L). To compare the results with nanotubes that have a similar length but are produced under static, bulk conditions, we fabricated TiO_2 nanotubes via the conventional electrochemical method and found that TiO_2 nanotubes generated in microfluidics showed significantly increased peak intensity of (004) (e.g., at 200 µL min^{-1}) (Figure 1L) and a ratio of peak intensity of (004) to (200), i.e., I_{004}/I_{200}, increased with flow rate (Figure 1M). The results suggest that the crystal growth of TiO_2 nanotubes produced at flow conditions is preferentially oriented along the [001] direction.[30,31] Collectively, the structural (e.g., length and diameter) and material (e.g., crystal orientation) properties of TiO_2 nanotubes can be controlled by changing the magnitude of flow rate in microfluidics during anodization.

We next examined the current–time characteristics of anodization under flow conditions (**Figure 2**A). Current–time curves particularly at high flow rate showed typical patterns of the anodic growth of TiO_2 nanotubes,[7] which included an exponential decrease of the current due to the formation of the oxide layer (stage I), followed by a slight increase of current due to the formation of initial porous structures (stage II), and then a relatively steady current due to the formation of self-organized nanotube arrays (stage III). The magnitude of the steady-state current at stage III correlates to the thickness of the nanotube arrays and will not increase significantly with extended anodization time unless the anodic potential is changed. Without the change of the applied voltage, however, we showed that the steady-state current changed with flow rate and increased linearly with Peclet number (Pe) (Figure 2B; Table S2, Supporting Information). Pe is defined as the ratio of the rate of convection by the flow to the rate of diffusion driven by a concentration gradient (Pe = Lu/D, where L is the smallest dimension of the channel, u is the flow velocity, and D is the diffusion coefficient) and high Pe indicates a convection-dominated mass transport process. Because the length of the nanotubes correlates with the steady-state current (Figure 2C), the increased steady-state current with Pe suggests that convective flow on the top of nanotube arrays must play a role in the regulation of key transport processes that are essential to the growth of TiO_2 nanotubes (Figure 2D).

Because previous studies of anodization of Ti in static conditions showed that there were concentration gradients of F^- and TiF_6^{2-} ions inside and outside the nanotube, and a diffusion layer was present adjacent to the top of the nanotubes,[10,16] the observed effects of flow on the growth of nanotubes is likely due to a convection-dominated mass transfer process. When flow is applied tangentially to the surface of nanotube arrays, for example, the thickness of the diffusion layer, L_{diff}, which can be estimated as $2\sqrt{Dt}$ or $2\sqrt{D\frac{L_{channel}}{u}}$ (where $L_{channel}$ is the length of the channel along the flow direction) decreases with the increase of flow velocity u and becomes negligible at high flow velocity or Pe. In this case, convection dominates the mass transport on the top of nanotube and local concentration of TiF_6^{2-} will approach to zero, and F^- concentration will be close to the bulk F^- concentration in the electrolyte (Figure 2D). The

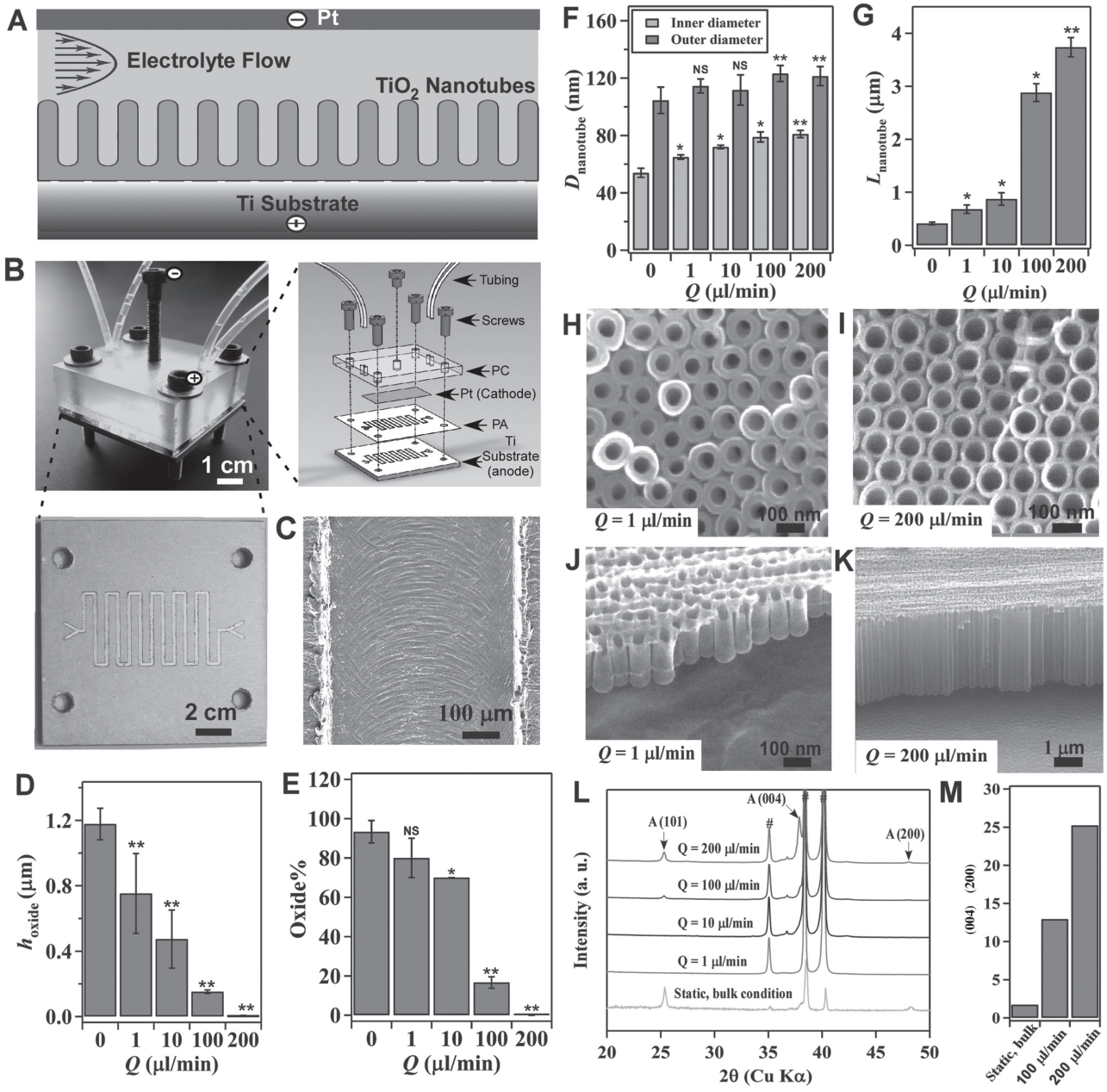

Figure 1. Flow in microfluidics controls the length, diameter, and crystal structures of TiO_2 nanotubes. A) Schematic of the generation of TiO_2 nanotubes via electrochemical anodization of Ti in microfluidics. B) A bright-field image of the assembled microfluidic device. Schematic image (right) shows the assembly of the microfluidic device using a titanium (Ti) substrate, a polyacrylate (PA) film, a Pt foil, and a block of polycarbonate (PC). The PA film acts as an isolating layer between the cathode (Pt) and the anode (Ti). The PC block serves as the cover of the microfluidic device. Four metal screws that are inserted through the corners of the PC block to the Ti substrate act as the anode electrodes. An additional screw that is inserted through the center of the device connects the Pt foil and serves as the cathode electrode. Enlarge image (below) shows the microfluidic channel fabricated on Ti by micromachining. The width and height of the channel are 500 and 50 μm, respectively. C) Representative SEM image of a TiO_2-nanotube-covered microfluidic channel. D) The change of thickness of the oxide layer, h_{oxide}, formed on the top of nanotube arrays with flow rate. E) Percentage of the coverage of the oxide layer at different flow rates in the microfluidic channel. F) Effect of flow rate on the inner and outer diameters of TiO_2 nanotubes. G) Effect of flow rate on the length of TiO_2 nanotubes. H,I) SEM images of top view of TiO_2 nanotubes fabricated at the flow rate of 1 and 200 μL min^{-1}, respectively. J,K) SEM images of side view of TiO_2 nanotubes fabricated at the flow rate of 1 and 200 μL min^{-1}, respectively. L) X-ray diffraction (XRD) patterns of annealed TiO_2 nanotubes. Nanotubes generated at the static conditon have a similar length as that produced at $Q = 200$ μL min^{-1}. Reflection peaks from Ti are labeled by #. M) Change of the peak intensity ratio of (004) to (200), I_{004}/I_{200}, at static and flow conditions.

change of local concentrations of TiF_6^{2-} and F^- on the top of nanotube modifies the boundary conditions of ion transport inside the nanotube where concentration gradients of F^- and TiF_6^{2-} still exist.[32] As a result, 1) ion-flux rates in the nanotube are enhanced in the presence of convective flow (Table S3, Supporting Information), resulting in an increased anodization current density with flow rate (Figure 2A). 2) Flow-induced change of ion transport could also affect the local electrical field during anodization and consequently influences the degree of preferred crystal orientation of

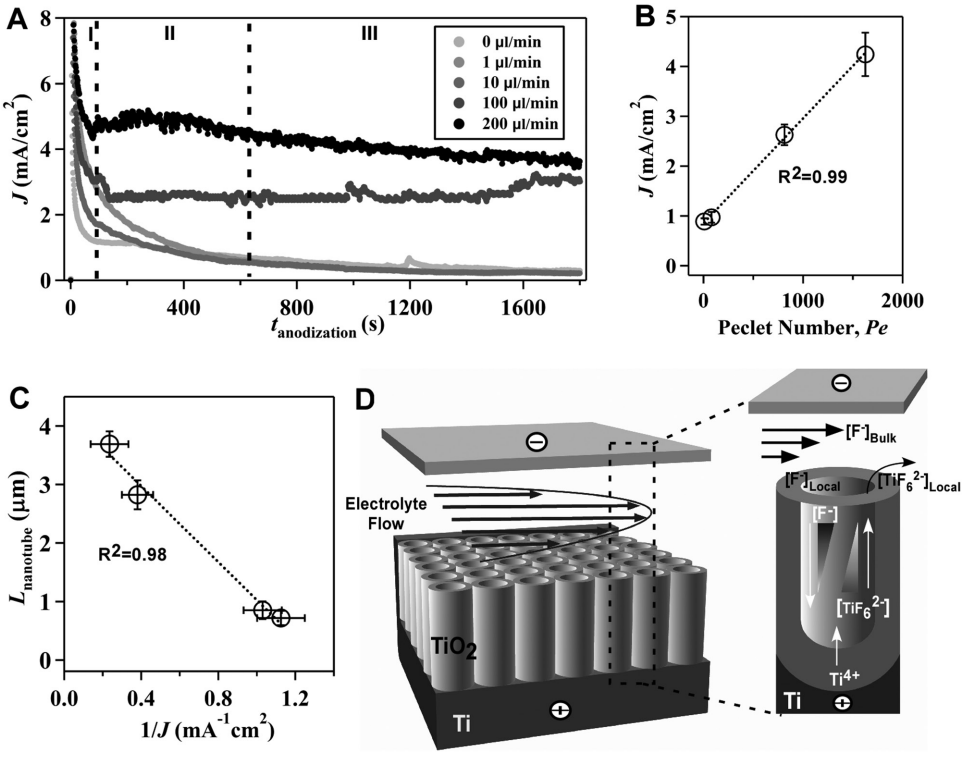

Figure 2. Flow regulates the current density during the anodic growth of TiO_2 nanotubes. A) Current–time curves during the growth of TiO_2 nanotubes at different flow rates. I, II, and III indicate different growth stages. Current density *J* is measured perpendicular to the flow direction. B) Steady current density at stage III increases linearly with Peclet number, Pe. Dotted line is a linear regression fitting curve with a correlation coefficient of 0.99. C) The length of TiO_2 nanotubes correlates reciprocally with the average steady current density. Dotted line is a linear regression fitting curve with a correlation coefficient of 0.98. D) Schematics of the regulatory roles of flow in the anodic growth of TiO_2 nanotubes. Flow at high Pe reduces the thickness of the diffusion layer on the top of the nanotube, and thus enhances ion flux inside the nanotube. In this case, $[F^-]_{Local} \approx [F^-]_{Bulk}$ and $[TiF_6^{2-}]_{Local} \approx 0$.

TiO_2 nanotubes upon annealing.[31] 3) Because TiF_6^{2-} is the diffusion-rate-controlling species in the formation of nanotubes,[12,16] effective removal of TiF_6^{2-} at high Pe accelerates the dissolution process occurring at the bottom of the nanotube, and thus produces long nanotubes in a short period of time (Figure 1G,K). 4) The increased concentration of F^- on the top of nanotubes facilitates the etching of the top nanotubes, leading to a large inner diameter (Figure 1I).

To further demonstrate the effect of flow on the growth of TiO_2 nanotubes, we changed the flow velocity profile and measured the diameter and length of nanotubes across the microfluidic channel perpendicular to the flow direction (**Figure 3**). When the height of the channel in the *z*-direction is larger than the width of the channel in the *y* direction, the velocity profile of the flow (in the *x*-direction) is parabolic in the *x*–*y* plane, with the highest flow velocity in the middle of the channel (Figure 3A). As a result, nanotubes in the middle of the channel are expected to have the largest inner diameter and length. Experimental results obtained at high flow rates were consistent with the prediction (Figure 3B–E). When we reduced the height of the channel while keeping the width of the channel unchanged, the parabolic flow profile switched from the *x*–*y* plane to the *x*–*z* plane, and left a relatively uniform velocity distribution in the *x*–*y* plane (Figure 3F). In this case, nanotubes with relatively uniform inner diameter and length across the channel were obtained (Figure 3G–J). Note that Pe or flow velocity was kept approximately the same in both devices (Tables S2 and S4, Supporting Information). Similar results were also obtained upstream and downstream in ends of the channel in both devices (Figures S4 and S5, Supporting Information). Our results thus show that the spatial distribution of nanotube structure in microfluidics can be controlled by manipulating the flow velocity profile during anodization.

When a metallic Ti thin film with a thickness of 500 nm was deposited on a conductive silicon substrate (Ω = 1–5 × 10^{-3} Ω cm) and patterned photolithographically inside a microfluidic channel (**Figure 4**A), we showed that TiO_2 nanotubes could grow uniformly inside the patterned areas (Figure 4B,C), and had an average diameter and length of 78 ± 5.4 and 304 ± 12.3 nm, respectively (Figure 4C). Intriguingly, when TiO_2 nanotubes were anodized microfluidically on a Ti thin film (1 μm thick) that was deposited on a nonconductive silicon substrate (Ω = 1–2 × 10^4 Ω cm) (Figure 4D,E), horizontally aligned nanotubes relative to the silicon substrate were produced inside the walls of the channel (Figure 4F), while vertically aligned nanotubes were present in the center of the channel (Figure 4G). Similar phenomena were observed using Ti layers with a reduced thickness or photolithographically patterned Ti layers (Figure S6, Supporting Information). The inner diameter and density of horizontally aligned nanotubes increased with flow rate (Figure 4H,I). We did not observe horizontally aligned nanotubes on a Ti layer that

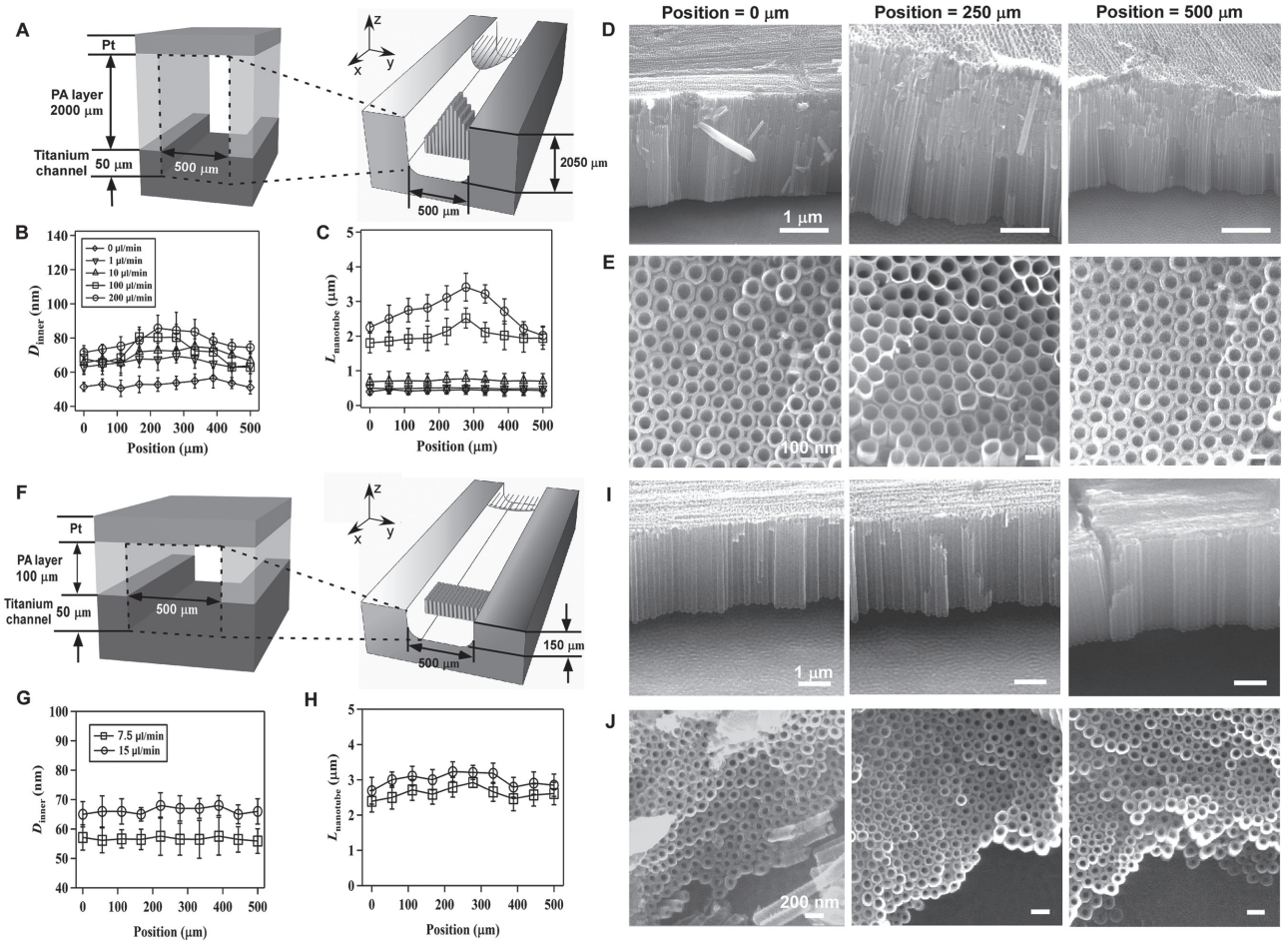

Figure 3. Flow velocity profile in microfluidics determines the spatial distribution of TiO_2 nanotubes. A) Schematics of the cross-sectional view of a microfluidic channel with a width of 500 μm and a height of 2050 μm. Because the height of the channel (in the *z*-direction) is much larger than the width of the channel (in the *y*-direction), the velocity profile of the flow (in the *x*-direction) is parabolic in the *x*–*y* plane. As a result, nanotubes with large inner diameter and length in the center of channel are expected. B,C) The change of inner diameter and length of TiO_2 nanotubes, respectively, across the width of the channel at different flow rates in a microfluidic device shown in panel (A). Panels (D) and (E) are side and top view SEM images of TiO_2 nanotubes, respectively, at different locations across the width of the channel. Channel height: 2050 μm. Flow rate: 200 μL min^{-1}. F) Schematics of the cross-sectional view of a microfluidic channel with a width of 500 μm and a height of 150 μm. In this case, the height of the channel is smaller than the width of the channel, the velocity profile of the flow is parabolic in the *x*–*z* plane, but flat in the *x*–*y* plane. Nanotubes with relatively uniform diameter and length across the channel width are expected. G,H) The change of inner diameter and length of TiO_2 nanotubes, respectively, across the width of a channel in a microfluidic device shown in panel (F). Panels (I) and (J) are side and top view SEM images of TiO_2 nanotubes, respectively, at different locations across the width of the channel. Channel height: 150 μm. Flow rate: 15 μL min^{-1}. Note that flow rates of 7.5 and 15 μL min^{-1} in device (F) provide the similar flow velocity or Pe as flow rates of 100 and 200 μL min^{-1} in device (A), respectively (Tables S2 and S4, Supporting Information).

was deposited on conductive silicon substrates (Figure S7, Supporting Information).

Because anodic growth of TiO_2 nanotubes follows the direction of the electrical field, the appearance of horizontally aligned nanotubes on nonconductive silicon substrates suggests that the direction of the electrical field switches to the horizontal direction relative to the silicon substrate during anodization. Indeed, when nanotubes grow throughout the entire Ti layer and reach the nonconductive silicon substrate at the late stage of anodization, the electrical field in the vertical direction will change to the horizontal direction due to the presence of a nonconductive silicon substrate at the bottom and the conductive Ti in the side walls (Figure 4J). Meanwhile, the growth of horizontally aligned TiO_2 nanotubes also requires the contact of Ti walls with the electrolyte solution so that field-aided reaction can penetrate into the Ti side walls to form nanotubes. Such Ti-electrolyte interaction is also likely at the late stage of anodization, considering the finite thickness of the Ti layer and the continuous chemical etching of the top of nanotube arrays. Evidently, at the end of anodization, the length of nanotubes inside the channel (376 ± 16.4 nm) was much smaller than the original thickness of the Ti layer (1 μm) (Figure S8, Supporting Information). Horizontally aligned nanotubes were not present at the early stage of anodization (5 min) (Figure S9, Supporting Information). Collectively, our results suggest that by controlling the direction of the applied electrical field and Ti-electrolyte interaction during anodization, TiO_2 nanotube arrays can be produced with desired orientations relative to the substrate.

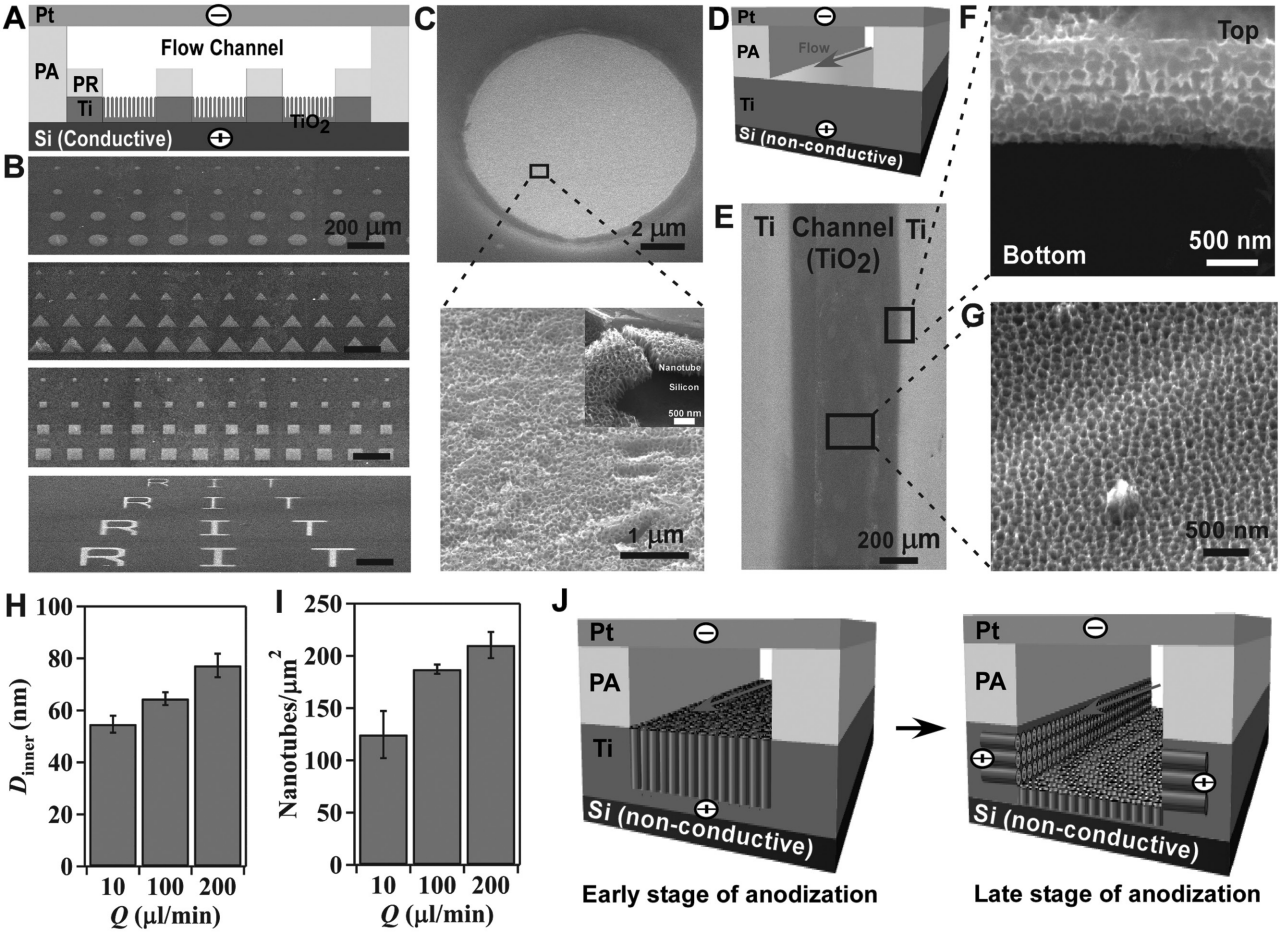

Figure 4. Controlled growth of TiO_2 nanotubes on silicon substrates. A) Schematic of the growth of TiO_2 nanotubes on a conductive silicon substrate ($\Omega = 1–5 \times 10^{-3}$ Ω cm) with photolithographically patterned goemetries. B) SEM images of TiO_2 nanotubes grown in patterned circles, triangles, squares, and letters of "RIT." C) High-resolution SEM images of TiO_2 nanotubes grown in a patterned circular shape. Images below show the top view and side view (inset) of TiO_2 nanotubes inside the circular pattern. D) Schematic of the growth of TiO_2 nanotubes on a nonconductive silicon substrate ($\Omega = 1–2 \times 10^4$ Ω cm). E) Representative SEM image of growing TiO_2 nanotubes on a nonconductive silicon substrate. The dark area indicates the channel where anodization occurs. The gray areas show Ti coated on silicon. F) SEM image of the edge of the channel where Ti in the wall was anodized to produce horizontally aligned TiO_2 nanotubes. G) SEM image of TiO_2 nanotubes growing in the center of the microfluidic channel. Panels (H) and (I) show, respectively, the change of inner diameter of horizontally aligned TiO_2 nanotubes, and the number of horizontally aligned TiO_2 nanotubes per area with flow rate. J) Schematics of the growth mechanism of horizontally aligned TiO_2 nanotubes on a nonconductive silicon substrate. The change of the direction of the electrical field and the exposure of Ti side walls to the electrolyte flow at the late stage of anodization likely contribute to the formation of horizontally aligned TiO_2 nanotubes.

In summary, we identified the regulatory roles of flow in the anodic growth of TiO_2 nanotube arrays in microfluidics, and showed that the structural, material, and spatial features of TiO_2 nanotubes can be controlled effectively in microfluidics. The microfluidic approach developed here offers a powerful platform to effectively grow oriented TiO_2 nanotubes, and a promising strategy to integrate silicon with hierarchical TiO_2 nanotube arrays that may find applications in nanoelectronics, silicon-based photonics, and photovoltaic solar cells.

Experimental Section

Details of the fabrication and assembly of microfluidic devices and the growth of TiO_2 nanotubes are described in the Supporting Information. A scanning electron microscope (FIB-SEM, Zeiss Cross Beam) was used to image the TiO_2 nanotubes. Nanotubes were etched with HCl (37%, Sigma-Aldrich) for 2–5 min and cleaned with acetone before imaging. Energy dispersive X-ray spectroscopy was conducted to analyze the presence of Ti and oxygen elements in the nanotubes. X-ray diffraction was conducted with a Philips X'Pert MRD diffractometer (Spectris PLC) using a long fine focus Cu Kα radiation source at 40 kV and 30 mA. The scanning range of 2θ was set from 20° to 50° with a 0.03° step size. The crystalline structures of TiO_2 nanotubes were identified by comparison and analysis with FIZ/NIST Inorganic Crystal Structure Database.

Supporting Information

Supporting Information is available from the Wiley Online Library or from the author.

Acknowledgements

The authors acknowledge the financial support from Rochester Institute of Technology (RIT), the New York State Energy Research and Development Authority (NYSERDA), NSF Award DMR 1461063 and REU Site: materials, application and development for organic photovoltaic devices. The authors thank Christiaan Richter and Howard Stone for constructive suggestions. The authors thank Christine Pratt and Surendra Gupta for XRD measurements. The authors also thank Patricia Taboada-Serrano, Xiang Li, and Xi Li for technical help. The authors thank Cornell Nanoscale Science and Technology Facility and RIT Machine Shop for device fabrication and Dan Xue for providing help on schematic figures.

Conflict of Interest

The authors declare potential conflict of interest with a patent in application.

[1] T. Close, G. Tulsyan, C. A. Diaz, S. J. Weinstein, C. Richter, *Nat. Nanotechnol.* **2015**, *10*, 418.
[2] V. Galstyan, E. Comini, G. Faglia, G. Sberveglieri, *Sensors* **2013**, *13*, 14813.
[3] I. Paramasivam, H. Jha, N. Liu, P. Schmuki, *Small* **2012**, *8*, 3073.
[4] C. Richter, C. A. Schmuttenmaer, *Nat. Nanotechnol.* **2010**, *5*, 769.
[5] P. Roy, D. Kim, K. Lee, E. Spiecker, P. Schmuki, *Nanoscale* **2010**, *2*, 45.
[6] G. K. Mor, O. K. Varghese, M. Paulose, K. Shankar, C. A. Grimes, *Sol. Energy Mater. Sol. Cells* **2006**, *90*, 2011.
[7] P. Roy, S. Berger, P. Schmuki, *Angew. Chem. Int. Ed.* **2011**, *50*, 2904.
[8] J. Macak, H. Tsuchiya, A. Ghicov, K. Yasuda, R. Hahn, S. Bauer, P. Schmuki, *Curr. Opin. Solid State Mater. Sci.* **2007**, *11*, 3.
[9] D. Regonini, C. Bowen, A. Jaroenworaluck, R. Stevens, *Mater. Sci. Eng., R* **2013**, *74*, 377.
[10] K. Yasuda, J. M. Macak, S. Berger, A. Ghicov, P. Schmuki, *J. Electrochem. Soc.* **2007**, *154*, C472.
[11] F. D. Aarao Reis, J. Badiali, D. di Caprio, *Langmuir* **2012**, *28*, 13034.
[12] J. Macak, H. Hildebrand, U. Marten-Jahns, P. Schmuki, *J. Electroanal. Chem.* **2008**, *621*, 254.
[13] S. Berger, J. Kunze, P. Schmuki, D. LeClere, A. T. Valota, P. Skeldon, G. E. Thompson, *Electrochim. Acta* **2009**, *54*, 5942.
[14] Y. Liang, Z. Cui, S. Zhu, X. Yang, *Thin Solid Films* **2011**, *519*, 5150.
[15] K. Deen, A. Farooq, M. Raza, W. Haider, *Electrochim. Acta* **2014**, *117*, 329.
[16] K. Yasuda, P. Schmuki, *Electrochim. Acta* **2007**, *52*, 4053.
[17] G. Mor, O. K. Varghese, M. Paulose, N. Mukherjee, C. A. Grimes, *J. Mater. Res.* **2003**, *18*, 2588.
[18] L. Taveira, J. Macak, H. Tsuchiya, L. Dick, P. Schmuki, *J. Electrochem. Soc.* **2005**, *152*, B405.
[19] S. P. Albu, A. Ghicov, S. Aldabergenova, P. Drechsel, D. LeClere, G. E. Thompson, J. M. Macak, P. Schmuki, *Adv. Mater.* **2008**, *20*, 4135.
[20] R. Beranek, H. Hildebrand, P. Schmuki, *Electrochem. Solid-State Lett.* **2003**, *6*, B12.
[21] Y. Y. Song, R. Lynch, D. Kim, P. Roy, P. Schmuki, *Electrochem. Solid-State Lett.* **2009**, *12*, C17.
[22] D. Kim, A. Ghicov, P. Schmuki, *Electrochem. Commun.* **2008**, *10*, 1835.
[23] J. Park, S. Bauer, K. von der Mark, P. Schmuki, *Nano Lett.* **2007**, *7*, 1686.
[24] S. P. Albu, A. Ghicov, J. M. Macak, R. Hahn, P. Schmuki, *Nano Lett.* **2007**, *7*, 1286.
[25] S. P. Albu, P. Schmuki, *Phys. Status Solidi RRL* **2010**, *4*, 151.
[26] J. H. Lim, J. Choi, *Small* **2007**, *3*, 1504.
[27] S. Bauer, S. Kleber, P. Schmuki, *Electrochem. Commun.* **2006**, *8*, 1321.
[28] M. Paulose, K. Shankar, S. Yoriya, H. E. Prakasam, O. K. Varghese, G. K. Mor, T. A. Latempa, A. Fitzgerald, C. A. Grimes, *J. Phys. Chem. Lett.* **2006**, *110*, 16179.
[29] S. P. Albu, A. Ghicov, P. Schmuki, *Phys. Status Solidi RRL* **2009**, *3*, 64.
[30] S. Lee, I. J. Park, D. H. Kim, W. M. Seong, D. W. Kim, G. S. Han, J. Y. Kim, H. S. Jung, K. S. Hong, *Energy Environ Sci.* **2012**, *5*, 7989.
[31] W. M. Seong, D. H. Kim, I. J. Park, G. D. Park, K. Kang, S. Lee, K. S. Hong, *J. Phys. Chem. C* **2015**, *119*, 13297.
[32] F. Thebault, B. Vuillemin, R. Oltra, J. Kunze, A. Seyeux, P. Schmuki, *Electrochem. Solid-State Lett.* **2009**, *12*, C5.

Received: April 10, 2017
Published online:

